

---

# Theoretical modelling of high-order harmonic generation

Ellipticity studies and extension to polar  
molecules

---

Adam Etches

...

Progress report

Lundbeck Foundation Theoretical Center for Quantum System Research  
Department of Physics and Astronomy  
Aarhus University  
12th May 2010.





---

# Contents

<b>Preface</b>	<b>iii</b>
<b>1 Introduction</b>	<b>1</b>
<b>2 High-order harmonic generation from molecules</b>	<b>3</b>
2.1 The Lewenstein model . . . . .	3
2.1.1 Deriving the Lewenstein model . . . . .	6
2.2 The stationary-phase method . . . . .	9
2.2.1 The standard stationary-phase method . . . . .	10
2.2.2 The extended stationary-phase method . . . . .	10
2.3 Elliptically polarized harmonics . . . . .	13
2.3.1 Calculating ellipticities . . . . .	13
2.3.2 Results . . . . .	14
<b>3 High-order harmonic generation from polar molecules</b>	<b>17</b>
3.1 Extending the Lewenstein model . . . . .	17
3.2 Gating mechanisms in HHG . . . . .	20
3.2.1 System-induced gating . . . . .	21
3.2.2 Field-induced gating . . . . .	23
3.2.3 Extending the harmonic cutoff . . . . .	24
<b>4 Conclusions and outlook</b>	<b>27</b>
4.1 Conclusions . . . . .	27
4.2 Outlook . . . . .	27
4.2.1 Structure determination for polar molecules . . . . .	28
4.2.2 Full momentum integral . . . . .	28
4.2.3 Propagation in the medium . . . . .	29

**Bibliography**

**30**



---

# Preface

This progress report sums up my work on high-order harmonic generation during the part A of my PhD studies at the Lundbeck Foundation Theoretical Center for Quantum Research at the Department of Physics and Astronomy, Aarhus University.

The first part of my studies was spent in close collaboration with Christian Bruun Madsen, who had previously studied high-order harmonic generation from molecules. This work resulted in an article illustrating the importance of including exchange orbits when evaluating the Lewenstein model of high-order harmonic generation [1]. The second part of my studies revolved around the problem of modelling polar molecules in intense laser fields. This work has also resulted in an article, which is currently being reviewed pending publication [2].

## Units

Atomic units ( $\hbar = e = m_e = a_0 = 1$ ) are used throughout unless stated otherwise.

## Acknowledgements

First of all I would like to thank my supervisor Lars Bojer Madsen. His focus on both the scientific and human aspects of doing a PhD is much appreciated. In my work on polar molecules I have had the pleasure of interacting with every single person in the New Light Sources group. Their patience and expertise has been a big help whenever I had an “unsolvable” problem.



---

# Introduction

Attosecond science is a new field, which is concerned with dynamics happening on the sub-femtosecond time scale. The major breakthroughs in attosecond science are due to the development of Ti:Sapphire lasers capable of delivering intense phase-stabilized few-cycle laser pulses in the near infrared spectrum. Peak intensities on the order of  $10^{13}$ – $10^{16}$  W/cm<sup>2</sup> lead to a range of multi-photon processes such as multi-photon ionization and high-order harmonic generation (HHG). The typical wavelength of the driving pulse is around 800 nm, which translates into roughly 3 femtoseconds per optical cycle. Multi-photon processes are very sensitive to the intensity of the electric field, leading to sub-cycle dynamics initiated at the peak of every half-cycle of the laser pulse. In this way the attosecond time scale is approached.

In HHG a target gas of atoms or molecules emits a very broad range of harmonics in response to an intense femtosecond laser pulse. High-order harmonic generation has attracted a great deal of interest as a potential table-top source of coherent attosecond pulses. Attosecond pulses opens up the possibility of following electron dynamics in molecules on their natural time scale. Another perspective is the generation of pulses with energies reaching into the water window (284–543 eV), which allows for detailed studies of, e.g., proteins inside cells.

It is extremely hard to perform *ab initio* calculations in strong-field physics. The main problem is that of dimensionality. Each new electron adds three dimensions to the physical system, thus greatly increasing the numerical challenge. State of the art *ab initio* codes are currently able to deal with the H<sub>2</sub><sup>+</sup> molecule. Another problem is that the natural electron time scale is attoseconds whereas the driving pulse is several femtoseconds. As the pulse is strong enough to greatly perturb the electronic states, this difference in time scales necessitates many time steps in numerical calculations.

With *ab initio* codes being unavailable for most target molecules used in experiments the need for modelling is apparent. The benchmark model of HHG is the

Lewenstein model [3], sometimes referred to as the strong-field approximation of HHG. It was originally developed for atomic targets, and has since been extended to molecules. Much effort has gone into determining when the Lewenstein model fails, and in extending it to include additional effects. The work presented here falls into both categories. In chapter 2 we first present part of the derivation of the Lewenstein model in order to clearly show which assumptions are made. We then show that the Lewenstein model predicts the appearance of elliptically polarized high-order harmonics from aligned molecules using a linearly polarized driving pulse [1]. This was previously thought not to be the case [4, 5]. In chapter 3 we show that the Lewenstein fails to describe HHG from polar molecules [2]. The reason for this is that the interaction between the field and the individual molecular orbitals causes a significant Stark shift. We propose an extension of the Lewenstein model in which this Stark shift is included, and illustrate its importance on the sub-cycle dynamics. In chapter 4 we sum up our findings and point at possible future topics of enquiry.



---

## High-order harmonic generation from molecules

High-order harmonic generation (HHG) takes place when an intense femtosecond laser pulse is focused onto a gas. The target atoms or molecules emit coherent radiation as harmonics of the driving field. The emitted harmonics all have a comparable intensity up until some cutoff, which is the signature of highly non-perturbative dynamics initiated by the strong laser. The harmonics are then phase-matched in the target medium resulting in a beam of high-order harmonics co-propagating with the driving pulse. A typical spectrum is shown in figure 2.1.

### 2.1 The Lewenstein model

One way of understanding HHG is by analogy with the radiation emitted by an accelerated classical point charge. The quantum mechanical equivalent is to calculate the time-dependent expectation value of the dipole acceleration. Another common model is the simple man's model [6]. The simple man's model describes HHG as three separate steps. In the first step an electron tunnels into the continuum due to the influence of the driving laser. In the second step the electron is accelerated away from its parent ion and back again when the electric field changes its sign. Finally, the electron recombines to its ground state and gets rid of its excess kinetic energy by emitting a single photon.

The two different ways of thinking about HHG are combined in the Lewenstein model [3]. The point of departure is to claim that the HHG spectrum  $S_{\mathbf{n}}(\omega)$  of the harmonic component along  $\mathbf{n}$  is given by

$$S_{\mathbf{n}}(\omega) = \left| \mathbf{n} \cdot \int e^{i\omega t} \frac{d}{dt} \langle \mathbf{v}_{\text{dip}}(t) \rangle dt \right|^2, \quad (2.1)$$

where  $\mathbf{v}_{\text{dip}}(t)$  is the dipole velocity. The geometry is sketched in figure 2.2. Equation (2.1) is the so-called *velocity form* of HHG. The *acceleration form* has the

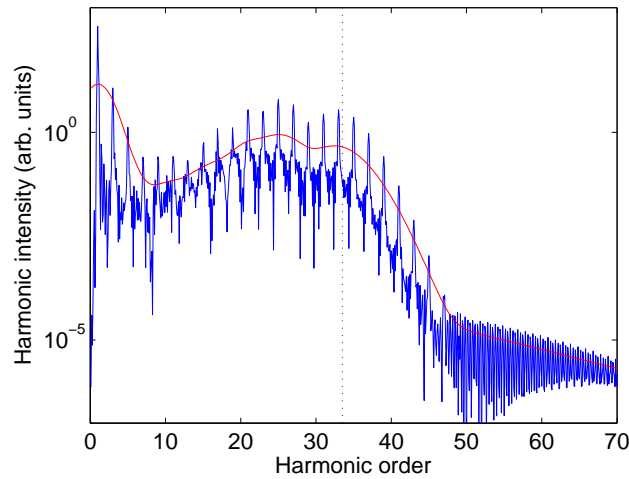


**Figure 2.1** | HHG spectrum from aligned CO calculated using the Lewenstein model. The driving pulse is fairly typical, with a central wavelength of 800 nm, eleven optical cycles in total, and a trapezoidal envelope with five optical cycles in the plateau. The peak intensity is  $2.0 \times 10^{14} \text{ W/cm}^2$ . The smooth (red) curve is obtained by averaging over neighbouring peaks. There is a characteristic plateau of harmonics of similar intensity leading up to the harmonic cutoff  $\omega_{\text{max}} = I_p + 3.17U_p$  indicated by the vertical broken line, where  $I_p$  is the vertical ionization potential and  $U_p$  the ponderomotive potential. It is also very typical that there are only odd harmonics in the spectrum due to the inversion symmetry of the target (alignment does not induce a head-to-tail direction) and driving field.

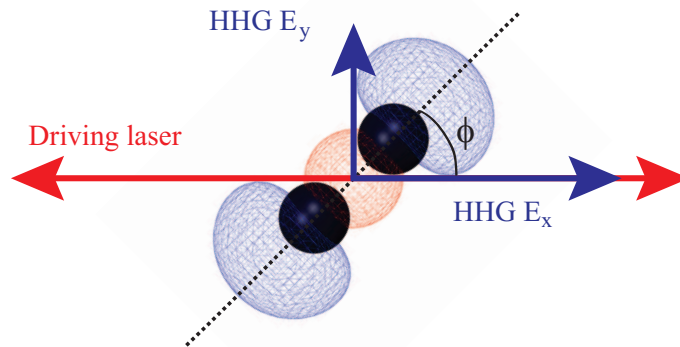


**Figure 2.2** | Sketch of the geometry in a HHG experiment. The laboratory frame is fixed by the driving pulse, which propagates along the  $z$  axis and is linearly polarized along the  $x$  axis. The target molecule is aligned in some way with respect to the laboratory frame. In this example it is an  $\text{N}_2$  molecule lying in the  $xy$  plane at an angle of  $\phi$  to the  $x$  axis. In general the emitted high-order harmonics will have a component which is parallel to the driving field and a component perpendicular to the driving field. The  $\text{N}_2$  molecule is indicated by its highest occupied molecular orbital (HOMO).

expectation value of the dipole acceleration. The *length form* has the double derivative of the dipole expectation value. The three forms are completely equivalent in an exact treatment, but vary slightly when approximations are introduced later on. We use the velocity form as it tends to reproduce experiments better than the two other forms [7]. Equation (2.1) does not include phase-matching and propagation effects in the gas medium. We will return to the question of medium effects in the outlook section of chapter 4.

The Lewenstein model itself amounts to a particular approximation of the dipole velocity in equation (2.1). The original Lewenstein model was derived for atoms [3], and it has been extended to the molecular case in various ways. My own work is a direct continuation of Christian Bruun Madsen's [8–12]. A complete description of the theory would take up too much space in this report, so some aspects of the theory will be assumed known with reference to Christian's progress report [11]. Other aspects will be described in higher detail, as they are necessary in order to understand my own recent work. First we write up the Lewenstein model in order to have all formulas collected in the same section.

At the time of the femtosecond driving pulse  $\mathbf{F}(t) = -\partial_t \mathbf{A}(t)$  the molecule is considered to be in its vibrational ground state, and have a given orientational distribution  $G(\mathcal{R})$  in the laboratory frame, where  $\mathcal{R}$  denotes the Euler angles  $\phi, \theta, \chi$  [13]. The orientational distribution is assumed to be fixed for the entire duration of the HHG driving pulse. We furthermore restrict ourselves to a single active electron. In this case the dipole velocity splits into a contribution from each molecular orbital  $\lambda$  [10]

$$\langle \mathbf{v}_{\text{dip}}(t) \rangle = \sum_{\lambda} P_{\lambda} \langle \mathbf{v}_{\lambda}(t) \rangle. \quad (2.2)$$

The orientational distribution  $G(\mathcal{R})$  of the molecule is factored out as a coherent sum [9, 10]

$$\langle \mathbf{v}_{\lambda}(t) \rangle = \int G(\mathcal{R}) \langle \mathbf{v}_{\lambda}(\mathcal{R}, t) \rangle d\mathcal{R}. \quad (2.3)$$

The Lewenstein model then states that the expectation value of the dipole velocity with respect to a perfectly oriented molecular orbital is

$$\begin{aligned} \langle \mathbf{v}_{\lambda}(\mathcal{R}, t) \rangle = & i \int_0^t d\tau \int d\mathbf{k} \mathbf{v}_{\text{rec},\lambda}^*(\mathcal{R}, \mathbf{k}, t) e^{-iS_{\lambda}(\mathbf{k}, t, t-\tau)} \\ & \times \mathbf{F}(t-\tau) \cdot \mathbf{d}_{\text{ion},\lambda}(\mathcal{R}, \mathbf{k}, t-\tau) \\ & + \text{complex conjugate}. \end{aligned} \quad (2.4)$$

The nuclear vibration is ignored, which is justified for heavy nuclei such as carbon, oxygen and nitrogen. For lighter nuclei the nuclear vibration can be included as in [8, 10, 11]. It is customary to restrict the  $\tau$ -integral from zero to a  $\tau_{\text{max}}$  of two thirds of an optical cycle. This selects the so-called short trajectories, which are the ones that dominate at the centre of the HHG beam in the far field.

Equation (2.4) may look complicated at first but actually has a very intuitive interpretation in terms of the three steps from the simple man's model. The first

step in which the electron tunnels into the continuum is described by the term

$$\mathbf{d}_{\text{ion},\lambda}(\mathbf{k}, t - \tau) = i\nabla_{\mathbf{k}+\mathbf{A}(t-\tau)}\tilde{\psi}_\lambda[\mathcal{R}, \mathbf{k} + \mathbf{A}(t - \tau)], \quad (2.5)$$

where  $\tilde{\psi}_\lambda$  denotes the Fourier transform of the electronic wave function. Propagation in the continuum is contained in the semi-classical phase factor

$$S_\lambda(\mathbf{k}, t, t - \tau) = \int_{t-\tau}^t \left( \frac{1}{2} [\mathbf{k} + \mathbf{A}(t'')]^2 - E_\lambda \right) dt'', \quad (2.6)$$

where  $|E_\lambda|$  is the vertical ionization potential of the molecular orbital in question. Finally, recombination back into the ground state is contained in the term

$$\mathbf{v}_{\text{rec},\lambda}(\mathbf{k}, t) = [\mathbf{k} + \mathbf{A}(t)]\tilde{\psi}_\lambda[\mathcal{R}, \mathbf{k} + \mathbf{A}(t)]. \quad (2.7)$$

### 2.1.1 Deriving the Lewenstein model

We will now show how the electronic part of the Lewenstein model can be derived using the theory of Green's functions. Nuclear motion has little impact on the results presented in this report, as nuclear motion in molecules like  $\text{N}_2$ ,  $\text{CO}_2$  and  $\text{CO}$  is negligible during the driving pulse. Furthermore, all orientational distributions are assumed to be perfect delta functions, making the coherent sum in equation (2.3) trivial for all non-polar molecules. The interested reader is referred to [11] for a treatment that includes both vibrational motion and orientational averaging.

The first step is to write the full electronic Hamiltonian as a sum of the field-free Hamiltonian  $\hat{H}_0$  and the interaction between the electron and the laser field

$$\hat{H} = \hat{H}_0 + V(t). \quad (2.8)$$

We choose the length gauge for interaction term [7]

$$V(t) = \mathbf{r} \cdot \mathbf{F}(t). \quad (2.9)$$

The field-free time-independent Schrödinger equation

$$\hat{H}_0 |\psi_\lambda^{(0)}\rangle = E_\lambda^{(0)} |\psi_\lambda^{(0)}\rangle \quad (2.10)$$

can be solved using quantum chemistry codes such as GAMESS-US [14]. In absence of any field the time-evolution is simply

$$|\psi_\lambda^{(0)}(t)\rangle = e^{-iE_\lambda^{(0)}(t-t_0)} |\psi_\lambda^{(0)}\rangle. \quad (2.11)$$

We now want to consider the effect that the laser has on the field-free eigenstates.

The solution to the full time-dependent Schrödinger equation can be written formally in terms of Green's functions. The Schrödinger equation is rewritten as an inhomogeneous differential equation

$$(i\partial_t - \hat{H}_0) |\psi_\lambda(t)\rangle = V(t) |\psi_\lambda(t)\rangle. \quad (2.12)$$

## Deriving the Lewenstein model

Equation (2.12) has the formal solution

$$|\psi_\lambda(t)\rangle = |\psi_\lambda^{(0)}(t)\rangle + \int_{-\infty}^{\infty} dt' G(t, t') V(t') |\psi_\lambda^{(0)}(t')\rangle, \quad (2.13)$$

where the Green's function  $G(t, t')$  is defined by

$$\left( i\partial_t - \hat{H} \right) G(t, t') = \delta(t - t'). \quad (2.14)$$

This postulate can be directly verified

$$\left( i\partial_t - \hat{H} \right) |\psi_\lambda(t)\rangle = \left( i\partial_t - \hat{H} \right) \left[ |\psi_\lambda^{(0)}(t)\rangle + \int_{-\infty}^{\infty} dt' G(t, t') V(t') |\psi_\lambda^{(0)}(t')\rangle \right] \quad (2.15)$$

$$= \left( i\partial_t - \hat{H}_0 \right) |\psi_\lambda^{(0)}(t)\rangle - V(t) |\psi_\lambda^{(0)}(t)\rangle \quad (2.16)$$

$$+ \int_{-\infty}^{\infty} dt' \left( i\partial_t - \hat{H} \right) G(t, t') V(t') |\psi_\lambda^{(0)}(t')\rangle \quad (2.17)$$

$$= -V(t) |\psi_\lambda^{(0)}(t)\rangle + \int_{-\infty}^{\infty} dt' \delta(t - t') V(t') |\psi_\lambda^{(0)}(t')\rangle \quad (2.18)$$

$$= -V(t) |\psi_\lambda^{(0)}(t)\rangle + V(t) |\psi_\lambda^{(0)}(t)\rangle \quad (2.19)$$

$$= 0 \quad (2.20)$$

If we somehow had access to all solutions of the full Hamiltonian

$$\left( i\partial_t - \hat{H} \right) |\psi_\xi(t)\rangle = 0 \quad (2.21)$$

then

$$G(t, t') = -i\Theta(t - t') \sum_{\xi} |\psi_\xi(t)\rangle \langle \psi_\xi(t')|, \quad (2.22)$$

where  $\Theta(t - t')$  is the Heaviside step function. The interpretation of this Green's function is quite clear. It is the propagator that projects a given state onto the basis states  $|\psi_\xi\rangle$  at time  $t'$  and evolves them in time up until time  $t$ . The role of the step function is to restrict time-evolution to the forward direction. The proof that equation (2.22) really gives the correct Green's function is to insert it in equation (2.14) and check

$$\left( i\partial_t - \hat{H} \right) G(t, t') = -i \left( i\partial_t - \hat{H} \right) \Theta(t - t') \sum_{\xi} |\psi_\xi(t)\rangle \langle \psi_\xi(t')| \quad (2.23)$$

$$= (\partial_t \Theta(t - t')) \sum_{\xi} |\psi_\xi(t)\rangle \langle \psi_\xi(t')| \quad (2.24)$$

$$- i\Theta(t - t') \sum_{\xi} \left( i\partial_t - \hat{H} \right) |\psi_\xi(t)\rangle \langle \psi_\xi(t')| \quad (2.25)$$

$$= \delta(t - t') \sum_{\xi} |\psi_\xi(t)\rangle \langle \psi_\xi(t')| - 0 \quad (2.26)$$

$$= \delta(t - t'). \quad (2.27)$$

The problem with equation (2.22) is that it involves the exact solutions to the full Schrödinger equation, which was exactly the problem that we wanted to solve in the first place. The way to get around this problem is to think of  $G(t, t')$  as the propagator, and use intuition gained from the simple man's model. In the simple man's model the electron tunnels into the continuum, and is then essentially uninfluenced by the molecular ion until it recombines. This means that its dynamics can be approximated using a Green's function  $G_{\text{vol}}(t, t')$  that only takes into account the continuum dynamics from the kinetic energy operator  $\hat{T}$  and the interaction with the laser field

$$\left(i\partial_t - \hat{T} - V(t)\right) G_{\text{vol}}(t, t') = \delta(t - t'). \quad (2.28)$$

Luckily there exists an analytical solution to a free electron in a vector potential. Let  $\mathbf{A}(t)$  define the intense femtosecond pulse  $\mathbf{F}(t) = -\partial_t \mathbf{A}(t)$  starting at time  $t_0$ . The solution is then the so-called Volkov wave

$$\psi_{\mathbf{k}}(\mathbf{r}, t) = (2\pi)^{-3/2} \exp\left(i\left[\mathbf{k} + \mathbf{A}(t)\right] \cdot \mathbf{r} - \int_{t_0}^t \frac{1}{2}(\mathbf{k} + \mathbf{A}(t'))^2 dt'\right). \quad (2.29)$$

Volkov waves are seen to be plane waves where the kinetic momentum  $\mathbf{k}$  has been replaced by the canonical momentum  $\mathbf{k} + \mathbf{A}(t)$ . Using these states yields the Volkov propagator

$$G_{\text{vol}}(t, t') = -i\Theta(t - t') \int d\mathbf{k} |\psi_{\mathbf{k}}(t)\rangle \langle \psi_{\mathbf{k}}(t')|. \quad (2.30)$$

The  $\mathbf{k}$  integral is a three-dimensional integral over all kinetic momenta. Plugging  $G_{\text{vol}}(t, t')$  into equation (2.13) yields

$$|\psi_{\lambda}(t)\rangle \approx |\psi_{\lambda}^{(0)}(t)\rangle + \int_{-\infty}^{\infty} dt' G_{\text{vol}}(t, t') V(t') |\psi_{\lambda}^{(0)}(t')\rangle \quad (2.31)$$

$$= |\psi_{\lambda}^{(0)}(t)\rangle - i \int_{-\infty}^t dt' \int d\mathbf{k} |\psi_{\mathbf{k}}(t)\rangle \langle \psi_{\mathbf{k}}(t')| V(t') |\psi_{\lambda}^{(0)}(t')\rangle \quad (2.32)$$

$$= |\psi_{\lambda}^{(0)}(t)\rangle - i \int_{t_0}^t dt' \int d\mathbf{k} |\psi_{\mathbf{k}}(t)\rangle \langle \psi_{\mathbf{k}}(t')| \mathbf{F}(t') \cdot \mathbf{r} |\psi_{\lambda}^{(0)}(t')\rangle. \quad (2.33)$$

In the final step the  $t'$  integral is restricted because the electric field is zero at times earlier than  $t_0$ .

The Lewenstein model now follows from equation (2.33) by taking the expectation value of the dipole velocity  $\mathbf{v} = -i\nabla$

$$\langle \mathbf{v}_{\lambda}(t) \rangle = \langle \psi_{\lambda}(t) | \mathbf{v} | \psi_{\lambda}(t) \rangle \quad (2.34)$$

$$\approx -i \int_{t_0}^t dt' \int d\mathbf{k} \langle \psi_{\lambda}^{(0)}(t) | \mathbf{v} | \psi_{\mathbf{k}}(t) \rangle \langle \psi_{\mathbf{k}}(t') | \mathbf{F}(t') \cdot \mathbf{r} | \psi_{\lambda}^{(0)}(t') \rangle \quad (2.35)$$

+ complex conjugate

Only the two cross terms are kept in (2.35). The direct term involving only  $|\psi_{\lambda}^{(0)}\rangle$  is exactly zero. The direct term involving matrix elements between Volkov states is very small due to a weak coupling between continuum states.

The derivation of the Lewenstein model as written in equation (2.35) is based on the expectation value of the dipole velocity with respect to an approximate time-dependent state. In this respect it supports a picture of HHG in which the emitted radiation is due to an oscillating dipole. The connection to the three steps of the simple man's model is regained when the terms in equation (2.35) are interpreted. First

$$\langle \psi_{\mathbf{k}}(t') | \mathbf{F}(t') \cdot \mathbf{r} | \psi_{\lambda}^{(0)}(t') \rangle \quad (2.36)$$

is the amplitude for ionizing from the molecular orbital  $|\psi_{\lambda}^{(0)}\rangle$  at time  $t'$  via the interaction with the laser field. This is the first step in the simple man's model. Propagation in the field enters through the time-evolution of the Volkov state from  $t'$  to  $t$

$$|\psi_{\mathbf{k}}(t)\rangle \langle \psi_{\mathbf{k}}(t')|. \quad (2.37)$$

In equation (2.4) this manifests itself as a semi-classical phase factor  $S_{\lambda}(\mathbf{k}, t, t')$ . The recombination step at time  $t$  is represented by the matrix element

$$\langle \psi_{\lambda}^{(0)}(t) | \mathbf{v} | \psi_{\mathbf{k}}(t) \rangle. \quad (2.38)$$

The momentum and time integrals in (2.35) ensure that the weight on all possible ionization times and continuum orbits are included. This way of thinking is directly inspired by Feynman path integrals, in which the orbits obtained from a stationary-phase approximation yield the classical limit. This will be the theme of the next section.

The Lewenstein model as written in equation (2.4) is obtained by writing all matrix elements in the position representation, and using the fact that taking the inner product with a plane wave is the same as taking the Fourier transform. This trick makes it numerically much cheaper to evaluate the Lewenstein model.

## 2.2 The stationary-phase method

The Lewenstein model is most conveniently calculated in the form of equation (2.4). In this form there are a total of five integrals. Three momentum integrals, one time integral, and one Fourier transform in equation (2.1). The Fourier transform is fast due to the fast Fourier transform routine, and does not pose any numerical problems. Evaluating the remaining four integrals is fairly expensive, however. One way around this is to use the stationary-phase method. The stationary-phase method can be used whenever the integrand splits into the product of a slowly varying function and a quickly oscillating phase factor. The quickly varying phase will average out all contributions from the integral except those at which the phase itself is slowly varying. This means that the total integral can be approximated with a normalization constant times the value of the integrand at the stationary point of the phase.

## 2.2.1 The standard stationary-phase method

Identifying the total phase with  $S_\lambda(\mathbf{k}, t, t - \tau)$  in equation (2.6) gives the stationary-phase condition

$$\nabla_{\mathbf{k}} S_\lambda(\mathbf{k}, t, t - \tau) \Big|_{\mathbf{k}=\mathbf{k}_s} = 0, \quad (2.39)$$

which leads directly to the stationary momentum

$$\mathbf{k}_s = -\frac{1}{\tau} \int_{t-\tau}^t \mathbf{A}(t'') dt''. \quad (2.40)$$

The stationary-phase method thus yields [15]

$$\begin{aligned} \langle \mathbf{v}_\lambda(\mathcal{R}, t) \rangle \approx & i \int_0^t d\tau \left( \frac{2\pi}{\epsilon + i\tau} \right)^{3/2} \mathbf{v}_{\text{rec},\lambda}^*(\mathcal{R}, \mathbf{k}_s, t) \\ & \times e^{-iS_\lambda(\mathbf{k}_s, t, t-\tau)} \mathbf{F}(t - \tau) \cdot \mathbf{d}_{\text{ion},\lambda}(\mathcal{R}, \mathbf{k}_s, t - \tau) \\ & + \text{complex conjugate.} \end{aligned} \quad (2.41)$$

Calculated spectra depend only weakly on the chosen value of  $\epsilon$ , which is set to 1.

The interpretation of the stationary-phase approximation is that only the most contributing Feynman paths in the continuum are kept. The contributing orbits are exactly the ones that result in the electron returning to the molecule at time  $t$ , which can be verified from equation (2.40). One important consequence is that the electron momentum is forced to follow the polarization axis of a linearly polarized laser pulse. Semi-classically this is because the electron only feels an acceleration parallel to the polarization axis, thus forcing any emitted harmonics to be polarized parallel to the laser. A more rigorous argument refers to equation (2.7), which shows that the recombination term  $\mathbf{v}_{\text{rec},\lambda}^*(\mathcal{R}, \mathbf{k}_s, t)$  follows  $\mathbf{k}_s$ . In short, the Lewenstein model coupled with the standard stationary-phase approximation only leads to harmonics that are polarized parallel to the polarization axis of the driving laser, irrespective of the molecular orientation.

## 2.2.2 The extended stationary-phase method

Recent experiments have shown that oriented molecules can emit elliptically polarized high-order harmonics when submitted to a linearly polarized driving pulse [5]. The picture to have in mind is that sketched in figure 2.3. It is the same geometry as in figure 2.2, but this time the polarization ellipse has been added. The main point is that the emitted harmonics generally have a non-vanishing polarization component perpendicular to the polarization of the laser. This is in direct contradiction with the prediction in section 2.2.1, and has been interpreted as a failing of the Lewenstein model itself [4, 5].

It turns out, however, that the standard stationary-phase approximation is only valid for atoms. The reason for this is that there is an additional phase factor in molecules due to the internuclear separation [15]. This is readily seen when the



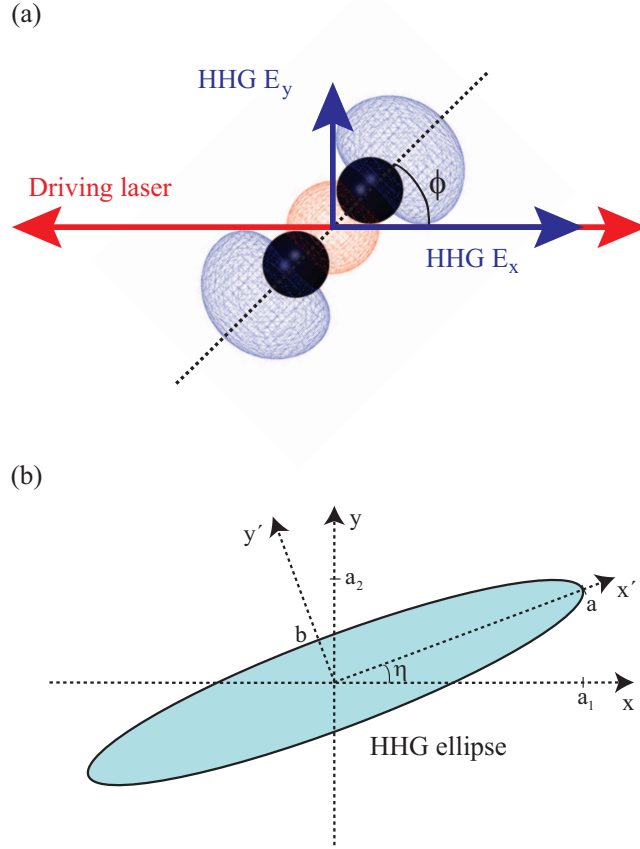


**Figure 2.3** | (a) An aligned molecule emits high-order harmonics with components  $E_x$  and  $E_y$  in response to a driving laser that is linearly polarized along the  $x$  axis. (b) The polarization ellipse for a single harmonic, where the two polarization components have been added up. The angle  $\eta$  of the major axis and the length  $b$  of the minor axis have been exaggerated for clarity.

electronic wave function is expanded around the atomic centers  $\mathbf{R}_n$  as

$$\psi_\lambda(\mathbf{r}) = \sum_n \phi_n(\mathbf{r} - \mathbf{R}_n). \quad (2.42)$$

Taking the Fourier transform yields

$$\tilde{\psi}_\lambda(\mathbf{k}) = (2\pi)^{-3/2} \int d\mathbf{r} e^{-i\mathbf{k}\cdot\mathbf{r}} \sum_n \phi_n(\mathbf{r} - \mathbf{R}_n) \quad (2.43)$$

$$= \sum_n e^{-i\mathbf{k}\cdot\mathbf{R}_n} (2\pi)^{-3/2} \int d\mathbf{r} e^{-i\mathbf{k}\cdot(\mathbf{r}-\mathbf{R}_n)} \phi_n(\mathbf{r} - \mathbf{R}_n) \quad (2.44)$$

$$= \sum_n e^{-i\mathbf{k}\cdot\mathbf{R}_n} \tilde{\phi}_n(\mathbf{k}) \quad (2.45)$$

This means that the Fourier transforms in equations (2.5) and (2.7) separate into terms each relating to just one atomic center

$$\mathbf{d}_{\text{ion},\lambda}(\mathbf{k}, t - \tau) = \sum_{n_i} \mathbf{d}_{\text{ion},\lambda}^{n_i}(\mathbf{k}, t - \tau), \quad (2.46)$$

and

$$\mathbf{v}_{\text{rec},\lambda}(\mathbf{k}, t) = \sum_{n_f} \mathbf{v}_{\text{rec},\lambda}^{n_f}(\mathbf{k}, t). \quad (2.47)$$

Each term in equation (2.46) and (2.47) acquires an associated phase factor  $e^{i[\mathbf{k}+\mathbf{A}(t-\tau)]\cdot\mathbf{R}_{n_i}}$  or  $e^{i[\mathbf{k}+\mathbf{A}(t)]\cdot\mathbf{R}_{n_f}}$  from equation (2.45), which has to be taken into account when performing the stationary-phase analysis. Here  $n_i$  refers to the atomic center involved in evaluating  $\mathbf{d}_{\text{ion},\lambda}^{n_i}$ , and  $n_f$  refers to  $\mathbf{v}_{\text{rec},\lambda}^{n_f}$ .

The above discussion means that equation (2.4) can be split into

$$\langle \mathbf{v}_\lambda(\mathcal{R}, t) \rangle = \sum_{n_i, n_f} \langle \mathbf{v}_\lambda^{n_i n_f}(\mathcal{R}, t) \rangle. \quad (2.48)$$

The stationary-phase condition for  $\langle \mathbf{v}_\lambda^{n_i n_f}(\mathcal{R}, t) \rangle$  is

$$\int_{t-\tau}^t (\mathbf{k} + \mathbf{A}(t'')) dt'' - (\mathbf{R}_{n_f} - \mathbf{R}_{n_i}) \Big|_{\mathbf{k}=\mathbf{k}_s} = 0, \quad (2.49)$$

with associated stationary momenta

$$\mathbf{k}_s^{n_i n_f} = -\frac{1}{\tau} \int_{t-\tau}^t \mathbf{A}(t'') dt'' + \frac{1}{\tau} (\mathbf{R}_{n_f} - \mathbf{R}_{n_i}). \quad (2.50)$$

Applying this multi-center stationary phase method to the integral in equation (2.4) finally yields

$$\begin{aligned} \langle \mathbf{v}_\lambda(\mathcal{R}, t) \rangle &\approx i \sum_{n_i n_f} \int_0^t d\tau \left( \frac{2\pi}{\epsilon + i\tau} \right)^{3/2} \mathbf{v}_{\text{rec},\lambda}^{n_f*}(\mathcal{R}, \mathbf{k}_s^{n_i n_f}, t) \\ &\times e^{-iS_\lambda(\mathbf{k}_s^{n_i n_f}, t, t-\tau)} \mathbf{F}(t-\tau) \cdot \mathbf{d}_{\text{ion},\lambda}^{n_i}(\mathcal{R}, \mathbf{k}_s^{n_i n_f}, t-\tau) \\ &+ \text{complex conjugate}. \end{aligned} \quad (2.51)$$

The terms in equation (2.51) can be interpreted as semi-classical orbits of electrons that are ionized at  $\mathbf{R}_{n_i}$  and recombine at  $\mathbf{R}_{n_f}$ . The effect of using the multi-center stationary phase method is to properly include orbits from one atom to another. In the case of diatomic molecules this gives rise to two different types of orbits, sketched in figure 2.4. The resulting harmonics are referred to as direct harmonics and exchange harmonics [15].

The exchange harmonics can contribute with a polarization component perpendicular to that of the driving laser if the molecule has a non-vanishing projection orthogonal to the driving laser. This can be understood in terms of accelerated charges or inferred from equations (2.7) and (2.50). The conventional stationary phase method only includes the direct harmonics, which is why the standard treatment of the Lewenstein model fails to produce elliptically polarized harmonics.

## Elliptically polarized harmonics

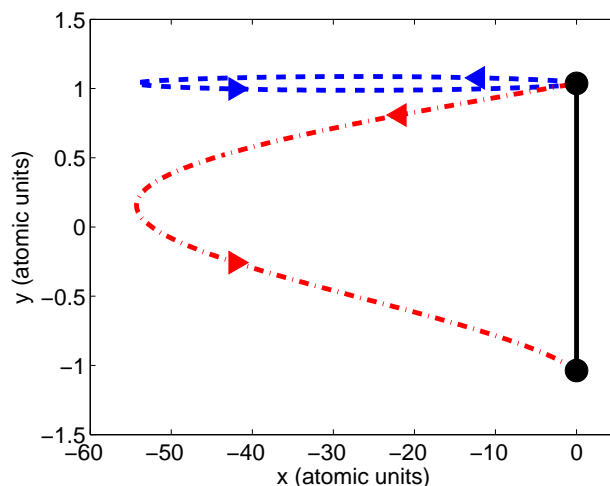


**Figure 2.4** | Two types of orbits with ionization at the peak of the field and recombination two thirds of an optical cycle later. The atomic centers of the molecule are sketched as black dots to the right. The laser polarization is taken to be in the  $x$  direction. The dashed (blue) line represents an orbit that gives rise to direct harmonics, i.e., ionization and recombination at the same center. A transverse component has been added manually to distinguish the return path. The dash-dotted (red) line is an orbit that gives rise to exchange harmonics, i.e., ionization at one center and recombination at another center. Note that the units on the two axis differ.

## 2.3 Elliptically polarized harmonics

The discussion in section 2.2.2 shows that the Lewenstein model in principle allows for elliptically polarized harmonics from an aligned molecule using a linearly polarized driving laser. The question remains, however, whether or not these actually do occur in our model calculations.

### 2.3.1 Calculating ellipticities

For the sake of completeness, we will briefly list the conventions used when calculating ellipticities from the output of our Lewenstein code. The code returns amplitudes for each alignment angle of the molecule in the laboratory frame

$$A_{\lambda,\mathbf{n}}(\omega) = \mathbf{n} \cdot \int e^{i\omega t} \frac{d}{dt} \langle \mathbf{v}_{\lambda}(\mathcal{R}, t) \rangle dt, \quad (2.52)$$

where  $\mathbf{n}$  is the unit vector in the  $x$  and  $y$  direction respectively. The harmonic signal is obtained from these as

$$S_{\lambda,\mathbf{n}}(\omega) = |A_{\lambda,\mathbf{n}}(\omega)|^2. \quad (2.53)$$

The amplitudes in equation (2.52) are born with a complex phase. We assume that the phase of the electric field component is the same as that of  $A_{\lambda,\mathbf{n}}(\omega)$  [16, 17].

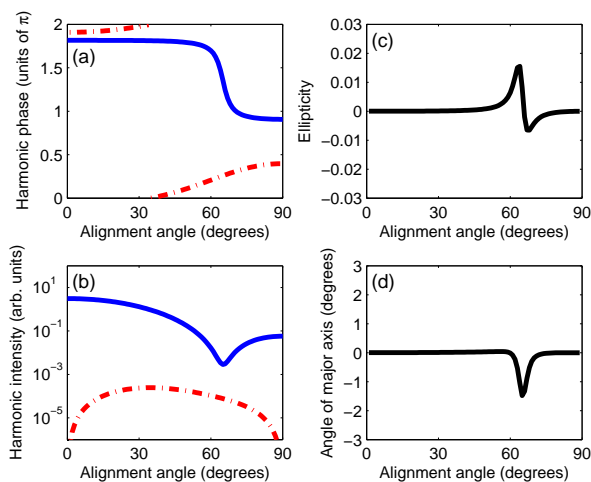


**Figure 2.5** | Orientation dependence of harmonic 17 from the  $3\sigma_g$  HOMO of  $N_2$  with equilibrium internuclear distance  $R_0 = 1.0977 \text{ \AA}$ . We use an 800 nm,  $6 \times 10^{14} \text{ W/cm}^2$  driving field. The envelope (for the vector potential) is trapezoidal with three optical cycles turn-on and turn-off and five cycles constant amplitude. (a) Harmonic phase (b) Harmonic intensity (c) Ellipticity (d) Angle of polarization ellipse major axis with respect to molecular axis. In (a) and (b) the solid (blue) curves refer to the parallel polarization component and the dash-dotted (red) curves to the perpendicular component.

We follow the conventions of [18] when calculating ellipticities. This means that the harmonic of angular frequency  $\omega$  is assumed to be a perfect plane wave

$$\mathbf{F}_{\text{HHG}}(t) = a_1 \cos(\omega t + \delta_1) \mathbf{e}_x + a_2 \cos(\omega t + \delta_2) \mathbf{e}_y \quad (2.54)$$

$$= a \cos(\omega t + \delta_0) \mathbf{e}_{x'} \pm b \sin(\omega t + \delta_0) \mathbf{e}_{y'}, \quad (2.55)$$

where  $\mathbf{e}_x, \mathbf{e}_y, a_1, a_2, \mathbf{e}_{x'}, \mathbf{e}_{y'}, a, b$  are defined in Fig. 2.3 (b). The two physically relevant quantities are the ellipticity  $\epsilon$ , and the angle  $\eta$  that the polarization ellipse major axis makes to the polarization axis of the driving pulse. These are determined by

$$\epsilon = \pm \frac{b}{a}, \quad -\frac{\pi}{4} \leq \tan^{-1}(\epsilon) \leq \frac{\pi}{4} \quad (2.56)$$

and

$$\tan(2\eta) = \frac{2a_1/a_2}{1 - (a_1/a_2)^2} \cos(\delta_2 - \delta_1). \quad (2.57)$$

### 2.3.2 Results

The following results are discussed in greater detail in [1]. We use  $N_2$  as our target molecule in order to be able to compare with experiments [5]. In order to keep the discussion as clear as possible we restrict ourselves to perfect alignments, ignore nuclear vibration, and only include the  $3\sigma_g$  orbital, which is the highest occupied molecular orbital (HOMO). The pulse parameters are chosen to mimic those

## Results

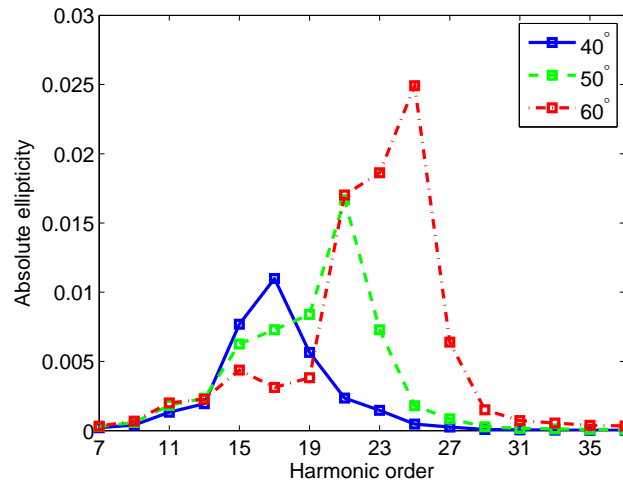


**Figure 2.6** | Absolute value of the harmonic ellipticity  $\epsilon$  as a function of harmonic order for selected alignment angles  $\phi$  of  $\text{N}_2$ . The solid (blue) curve refers to  $\phi = 40^\circ$ , the dashed (green) curve to  $\phi = 50^\circ$ , and the dash-dotted (red) curve to  $\phi = 60^\circ$ .

in the experiment [5]. This means choosing an 800 nm pulse with eleven optical cycles. The pulse envelope is taken to be trapezoidal, with five optical cycles with constant amplitude. Our peak intensity had to be chosen slightly higher than the  $2 \times 10^{14} \text{ W/cm}^2$  in the experiment due to technical problems arising from the discontinuous first derivative of the pulse envelope. Because HHG scales very favorably with field intensity, the higher intensity effectively blocks out any contribution away from the plateau of the envelope. A suitable intensity is  $6 \times 10^{14} \text{ W/cm}^2$ .

Figure 2.5 shows data for harmonic 17, with solid (blue) curves referring to the component parallel with the linear polarization of the driving field and dashed (red) curves to the perpendicular component. Panel (a) illustrates how the parallel polarization component of the harmonic emission changes its phase much faster than the perpendicular component. Comparison with panel (b) shows that the rapid change in phase is accompanied by a drop in harmonic intensity, causing an increase in the ratio of perpendicular to parallel harmonic intensity. From these it is possible to calculate the ellipticity and the angle of the major axis from figure 2.3. The result is shown in panel (c) and (d). Another way of viewing the ellipticity is as a function of harmonic for a fixed alignment angle as in figure 2.6.

Our calculations clearly show that the Lewenstein model does predict elliptically polarized harmonics from aligned  $\text{N}_2$ . Our ellipticities are an order of magnitude lower than those measured in the experiment, however. In our calculations the nature of the ellipticity is determined by the dip in the intensity of the parallel component as in figure 2.5. The dip in our data can be entirely understood in terms of a two-centre interference model [19]. In this model each nuclear site acts as a point emitter. At certain wave lengths the emitted harmonics from each centre will interfere destructively. Increasing the internuclear separation does not change the perpendicular component significantly but just changes the interference condition

in the two-centre interference model.

We have not tested whether our model agrees better with experiment if we include the HOMO–1 orbital [20] or a realistic alignment distribution. The main point is that the Lewenstein model does contain physical information on phenomena such as the occurrence of elliptically polarized harmonics, which is thrown away if the standard stationary-phase method is employed in evaluating the momentum integral. The success of the extended stationary-phase method is that it includes the exchange orbits starting at one nuclear centre and ending at another. This implies that correlations between the ionization and recombination step might be important when modelling HHG. Such a correlation is thrown away in some models that aim at extending the Lewenstein model to include the effect of the molecular ion on the continuum electron [20, 21].

---

## High-order harmonic generation from polar molecules

The Lewenstein model has been very successful in describing HHG. The crucial step in its derivation is to approximate the full electronic propagator with the Volkov propagator

$$G_{\text{vol}}(t, t') = -i\Theta(t - t') \int d\mathbf{k} |\psi_{\mathbf{k}}(t)\rangle \langle \psi_{\mathbf{k}}(t')| \quad (3.1)$$

describing the time-evolution of a free electron in a laser field from time  $t'$  to  $t$ . This approximation means that the time-evolution of a molecular orbital is given by

$$\begin{aligned} |\psi_{\lambda}(t)\rangle &= e^{-iE_{\lambda}(t-t_0)} |\psi_{\lambda}(t_0)\rangle - i \int d\mathbf{k} \int_{t_0}^t dt' |\psi_{\mathbf{k}}(t)\rangle \\ &\quad \times e^{-iE_{\lambda}(t'-t_0)} \langle \psi_{\mathbf{k}}(t') | \mathbf{F}(t') \cdot \mathbf{r} | \psi_{\lambda}(t_0)\rangle. \end{aligned} \quad (3.2)$$

This model completely ignores the effect of the molecular ion on the continuum electron as well as the effect of the laser field on the molecular orbitals of the molecule and the molecular ion. There has been quite a lot of interest in patching the Lewenstein model in order to include these effects. The main venue of investigation has been to include the Coulomb force in the continuum dynamics [20, 21]. There has also been some work on field dressing, where the molecular orbitals are coupled by the field [22].

### 3.1 Extending the Lewenstein model

Our approach to extending the Lewenstein model is inspired by recent work on strong-field ionization of polar molecules. It turns out that it is necessary to include the Stark shift felt by the molecular orbitals in order to understand the experimentally measured photoelectron angular distribution from oriented OCS [23]. Strong-field ionization and HHG are competing processes in many strong-field experiments. The photoelectron angular distribution can be obtained by projecting the

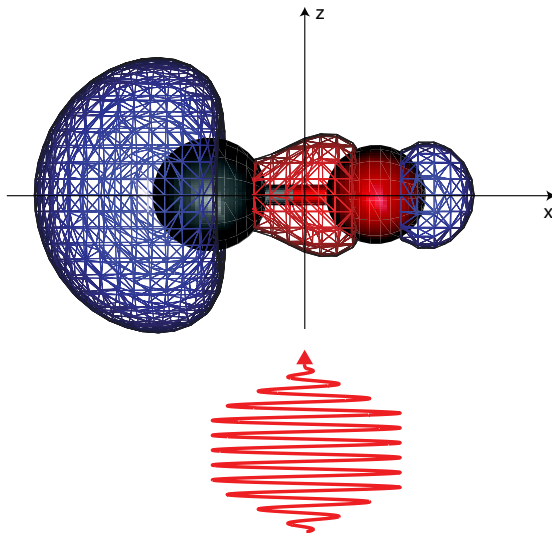


**Figure 3.1** | A sketch of the geometry. The molecule is oriented along the  $x$  axis, which is also the polarization axis of the linearly polarized driving pulse. Shown is the HOMO of CO. There is a larger electron density near the carbon nucleus to the left, leading to a dipole of 1.1287 a.u. pointing from the carbon to the oxygen nucleus. Note that the total dipole of the CO molecule is 0.112 D = 0.0441 a.u. pointing from the oxygen to the carbon nucleus.

time-dependent state (3.2) onto plane wave states. The HHG signal is obtained by calculating the time-dependent dipole acceleration with respect to (3.2). It therefore seems likely that the Stark shift also plays a role in HHG.

The phase factors in (3.2) containing  $E_\lambda$  are the result of applying the field-free time-evolution operator on a field-free energy eigenstate

$$|\psi_\lambda^{(0)}(t)\rangle = \exp\left(-i \int_{t_0}^t \hat{H}_0 dt'\right) |\psi_\lambda(t_0)\rangle \quad (3.3)$$

$$= e^{-iE_\lambda(t-t_0)} |\psi_\lambda(t_0)\rangle. \quad (3.4)$$

Referring to the formal solution in equation (2.13), the field-free time-evolution does not introduce any approximations in our model, as the entire influence of the driving laser is included in the propagator  $G(t, t')$ . This nice picture is ruined when we approximate the propagator with the Volkov propagator in equation (3.1). The reason is that the Volkov states  $|\psi_{\mathbf{k}}\rangle$  only account for the effect of the laser field on the continuum electron. The effect of the laser field on the molecule and molecular ion is neglected, as is the effect of the molecular ion on the continuum electron.

The strategy is now to reintroduce the effect of the field on the molecule. It is easy to see why this is necessary. Any field-free eigenstate will experience a Stark



## Extending the Lewenstein model

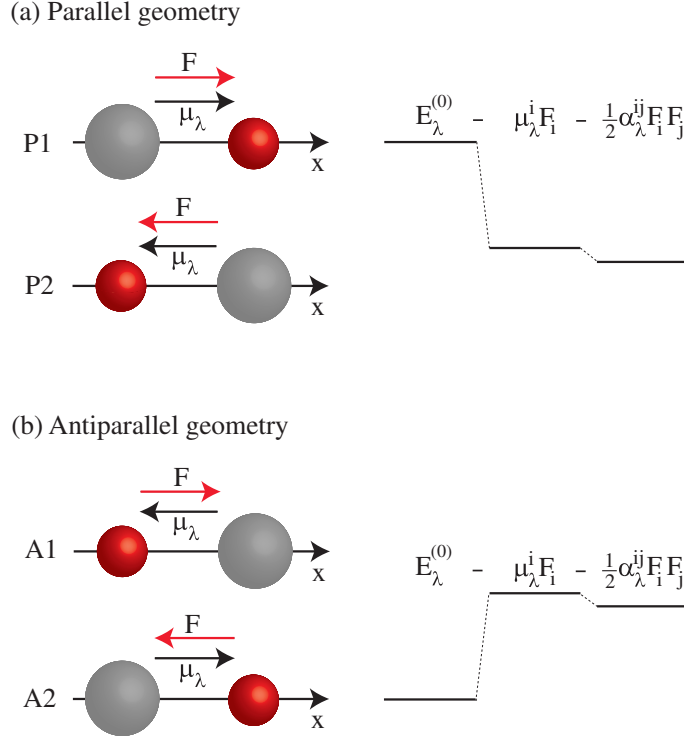


**Figure 3.2** | The two possible orientations of CO with the associated Stark shifts drawn to scale using the maximal field strength and the molecular parameters from the text. The nuclei are drawn with an unequal size (C being the larger) to reflect the charge distribution of the HOMO in figure 3.1. (a) The HOMO dipole  $\mu_\lambda$  is parallel to the electric field  $F$  so the energy of the HOMO  $E_\lambda$  is shifted down. (b) The antiparallel geometry, in which the HOMO is shifted up in energy. The second-order induced-dipole shift caused by the polarizability  $\alpha_\lambda$  is independent of the orientation, and is much smaller than the first-order shift.

shift in response to an electric field  $\mathbf{F}$ . Expanding in powers of the field, the shifted energy reads

$$E_\lambda = E_\lambda^{(0)} - \mu_\lambda^i F_i - \frac{1}{2} \alpha_\lambda^{ij} F_i F_j - \frac{1}{3!} \beta_\lambda^{ijk} F_i F_j F_k - \dots \quad (3.5)$$

where  $\mu_\lambda$  is the dipole,  $\alpha_\lambda$  the polarizability and  $\beta_\lambda$  the first hyperpolarizability of the molecular orbital expressed in the laboratory frame. We use Einstein summation for the tensor products. Taking CO as an example, the highest occupied molecular orbital (HOMO) in figure 3.1 experiences an energy shift of 17% using typical pulse parameters. The size and direction of the shift is shown in figure 3.2.

We propose to extend the Lewenstein model by Stark shifting the molecular orbitals according to the instantaneous value of the electric field [2]

$$E_\lambda(t) = E_\lambda^{(0)} - \mu_\lambda^i F^i(t) - \frac{1}{2} \alpha_\lambda^{ij} F_i(t) F_j(t) - \dots \quad (3.6)$$

In this quasi-static approximation it then follows that

$$e^{-iE_\lambda(t-t_0)} |\psi_\lambda(t_0)\rangle \rightarrow \exp\left(-i \int_{t_0}^t E_\lambda(t') dt'\right) |\psi_\lambda(t_0)\rangle. \quad (3.7)$$

The appealing feature of our approach is that it leaves the Lewenstein model in chapter 2 essentially unchanged. The only difference is that  $E_\lambda$  has to be replaced by  $E_\lambda(t)$ . The energy only enters in the semi-classical phase  $S$  in equation (2.6). The net effect is thus to introduce a time-dependent ionization potential. The dipole and polarizabilities are found by calculating the energy of each molecular orbital for a range of static field strengths using GAMESS-US [14], and fitting the result to a polynomial.

Our model is expected to be valid in the regime where the higher-order Stark shifts are small. In HHG experiments typical field intensities are of the order of  $1\text{--}2 \times 10^{14}$  W/cm<sup>2</sup>, corresponding to a maximal field-strength of

$$F_0 \approx \sqrt{2 \times 10^{14} / 3.51 \times 10^{16}} \text{ a.u.} \quad (3.8)$$

$$= 0.075 \text{ a.u.} \quad (3.9)$$

Sticking to CO as an example, our quantum chemistry calculations [14] show that the HOMO, sketched in figure 3.1, has a permanent dipole of 1.1287 a.u. leading to a Stark shift of 17% of the ionization potential. The maximal Stark shift is shown in figure 3.2 for the two possible orientations. The second-order Stark shift is much smaller than the first-order shift indicating that the field does not induce a large deformation of the molecular orbital or, equivalently, that there is not a large degree of state mixing of the bound states.

Simple considerations show why it has not previously been necessary to include the Stark shift in HHG modelling. The term that is linear in the field will always be exactly zero for non-polar molecules as their molecular orbitals do not possess a permanent dipole. The second-order term is symmetric with respect to the sign of the field and thus does not distinguish between half-cycles, and higher-order terms are heavily suppressed due to the typical size of  $F_0$  in HHG studies. The net effect is a slight lowering of the energy at the peak of the cycle due to the second-order Stark shift, leading to a negligible suppression of the total HHG signal. Including the first-order Stark shift is important for polar target molecules, however. The effect of the Stark shift on the sub-cycle dynamics of HHG is conveniently discussed in the context of gating mechanisms.

## 3.2 Gating mechanisms in HHG

The detailed shape of HHG spectra vary widely depending on the laser parameters of the driving pulse and the chosen target. One feature is very common, though. Almost all spectra consist solely of odd harmonics of the driving field. Any other spectral components are the result of schemes deliberately aiming at generating them. One way to understand the dominance of odd harmonics is in terms of Fourier components. Typical linearly polarized driving fields consist of enough optical cycles to be considered essentially inversion symmetric. Targets consisting of atoms or aligned molecules are also inversion symmetric. This means that the electronic dipole  $\mathbf{d}(t)$  will follow the sign of the electric field [24]. In other words

$$\mathbf{d}(t + T/2) = -\mathbf{d}(t), \quad (3.10)$$

where  $T$  is the duration of one optical cycle. Any even Fourier component cancels out because

$$e^{-i2n\omega(t+T/2)} = e^{-i2n\omega t} e^{-in\omega T} \quad (3.11)$$

$$= e^{-i2n\omega t}. \quad (3.12)$$

Any odd Fourier component survives because

$$e^{-i(2n+1)\omega(t+T/2)} = e^{-i(2n+1)\omega t} e^{-i(n+1/2)\omega T} \quad (3.13)$$

$$= -e^{-i(2n+1)\omega t}. \quad (3.14)$$

In order to generate even harmonics it is necessary to break the symmetry of either the target or the driving field. Breaking the inversion symmetry of the target molecule is made possible, e.g., by recent advances in field-free molecular orientation [23, 25–27]. As opposed to aligned molecules, that only have a well-defined internuclear axis, oriented molecules also have a well-defined head-to-tail direction. In general, such a molecule will have a preferred direction of ionization [23, 28], which means that the harmonic contribution will be larger from one half-cycle than the adjacent. We refer to this gating mechanism, as *system-induced gating* as it is the molecule itself that serves as a gate. We show that the Stark shift tends to decrease the strength of system-induced gating.

We also consider *field-induced gating*, in which it is the symmetry of the driving laser that is broken. Another way of putting this is to say that the waveform is changed so as to dampen the harmonic emission from an aligned target in every other half-cycle. An easy way to implement field-induced gating is to add a small amount of the second harmonic of the driving laser to the driving pulse [29–31]. The second harmonic will dampen (enhance) every other half-cycle, thus damping (enhancing) the harmonic emission. We show that the Stark shift plays an important role in determining the relative HHG contribution from opposite orientations of the aligned molecule.

### 3.2.1 System-induced gating

The first gating mechanism to be discussed is system-induced gating, where the symmetry between half-cycles in HHG is broken due to a preferred direction of ionization in the oriented target molecule [23, 28]. One possible cause of asymmetry is the asymmetric charge distribution of the molecular orbital. Such a charge distribution necessarily leads to an asymmetry between half-cycles within the Lewenstein model. The argument for this relies on the standard stationary-phase method in section 2.2.1, and is presented in full in [2]. It has been omitted here as it is not essential for the further discussion. In short, the asymmetric charge distribution always leads to a suppression of HHG from half-cycles in which the electric field is antiparallel to the permanent dipole of the molecular orbital. In the case of CO in figure 3.1, this corresponds to the field pointing in the negative  $x$  direction, thus trying to pull electronic charge in the positive  $x$  direction. This suppression can

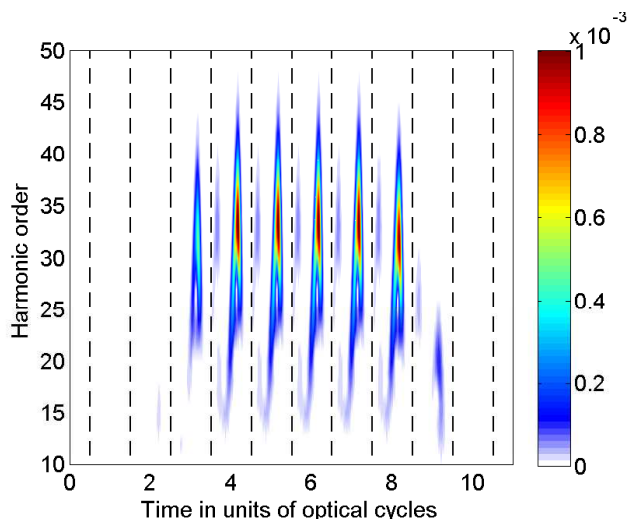


**Figure 3.3** | Gabor analysis illustrating system-induced gating when the Stark shift is omitted in (2.6). The driving field is an 800 nm pulse with eleven optical cycles and five optical cycles in the plateau. The peak intensity is  $2.0 \times 10^{14}$  W/cm<sup>2</sup>. The molecular target is the HOMO of CO oriented as in figure 3.1. The vertical dashed lines indicate the times at which the electric field peaks in the positive  $x$  direction. It is clearly seen that harmonic emission is restricted to once every other half-cycle due to the asymmetry of the target.

be intuitively understood as a screening effect, where the main effect of the charge on the oxygen nucleus is to prevent tunnelling in the positive  $x$  direction. These observations are confirmed by numerical results.

A common way of analyzing HHG is to perform a Gabor transform [32–34]. A plot of the Gabor transform yields information on the time at which a given harmonic is emitted. Figure 3.3 shows such a plot for oriented CO without inclusion of the Stark shift given the orientation in figure 3.1. The times at which the electric field peaks in the positive  $x$  direction are indicated by vertical dashed lines. As seen from the figure, harmonics are predominantly emitted every other half-cycle, corresponding to ionization in the positive half-cycle, and recombination roughly two thirds of an optical cycle later. Due to the asymmetry of the HOMO, the molecule itself acts as a gate for the HHG process.

The geometric effect always favours the parallel geometry in figure 3.2(a). The Stark effect, however, increases the effective ionization potential in the parallel geometry, resulting in a weakening of the system-induced gating. Figure 3.4 shows the Gabor analysis when the Stark shift is included in the semi-classical phase in (2.6) using equation (3.6). It is immediately clear that half-cycles suppressed in figure 3.3 now contribute much more strongly. Another way of saying this is that the sub-cycle dynamics is strongly influenced by the effect of the driving field on the molecular orbital. This influence is completely ignored in the regular Lewenstein model.

Spectra obtained with and without the Stark shift (not shown) exhibit differences in the detailed structure but it is difficult to make any quantitative comparison. Roughly speaking, the spectrum for oriented CO is more rugged when the Stark

## Field-induced gating

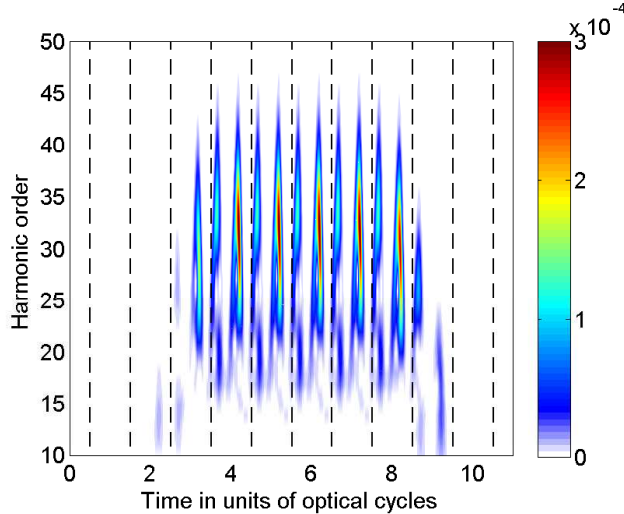


**Figure 3.4** | Gabor analysis illustrating the weakening of system-induced gating caused by the Stark shift. All parameters are the same as in figure 3.3 except that the Stark shift is now included in (2.6) using (3.6) for  $E(t)$ .

shift is included. This can be understood as a consequence of added interference between half-cycles.

### 3.2.2 Field-induced gating

Field-induced gating refers to any gating mechanism, which relies on a waveform that deviates from a pure sinusoidal field. One example is the use of pulses that are so short that tuning the carrier envelope phase allows for the selection of one particular half-cycle [35]. Another example is that of using a polarization gate, where only part of the pulse has a linear polarization that allows the ionized electron to recombine with the molecular ion [36, 37].

We will restrict ourselves to a very simple field-induced gating scheme. Adding a small fraction of the second harmonic to the driving pulse with a relative carrier-envelope phase delay of zero leads to every other peak in the resulting field being enhanced (suppressed) as illustrated in figure 3.5. Being initiated by tunnel ionization, HHG scales exponentially with the maximal field strength, making it possible to effectively weaken the HHG contribution from every other half-cycle. The control parameter is the amount of second harmonic that is added to the fundamental field.

In field-induced gating the target system is assumed to be inversion symmetric along the polarization axis. This means that polar molecules are only aligned, not oriented. An aligned molecule is the coherent superposition of two antiparallel oriented molecules so by equation (2.3) the total HHG signal is a coherent sum of the individual signals [9]. At a given half-cycle, each orientation will experience either a parallel or an antiparallel electric field leading to system-induced gating as described in section 3.2.1. Assuming that the Stark shift is negligible, and referring to the orientations in figure 3.2, P1 will dominate over A1 in the positive half-cycle, and P2

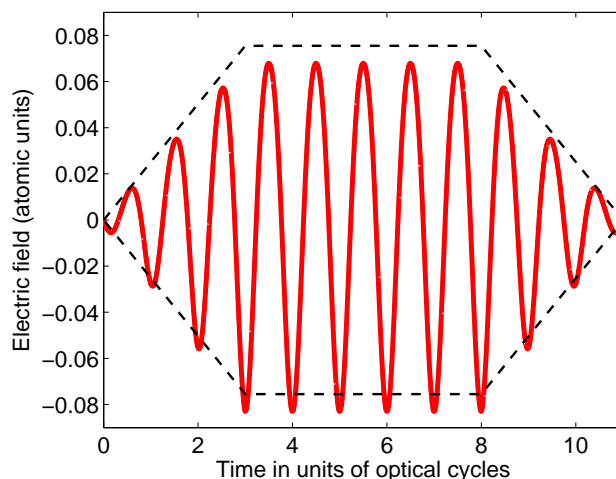


**Figure 3.5** | The result of adding 1% of the second harmonic in terms of intensity to an eleven cycle laser pulse with a trapezoidal envelope (indicated by the dashed line). The carrier envelope phase delay is set to zero in order to dampen (enhance) every other half-cycle.

will dominate over A2 in the negative half-cycle. The gating felt by each orientation is thus reversed in neighbouring half-cycles, ensuring the overall inversion symmetry of the HHG process.

The symmetry between the two orientations is broken in field-induced gating due to the broken symmetry of the electric field. This is clearly seen in figure 3.6, which shows a Gabor analysis of the two orientations. One orientation, figure 3.6(a), is seen to have its system-induced gating *counteracted* by the field-induced gating, and the other orientation, figure 3.6(b), to have its system-induced gating *enhanced*. The exact weight on each orientation is determined by the effectiveness of the system-induced gating, which depends on the Stark shift.

### 3.2.3 Extending the harmonic cutoff

System-induced and field-induced gating work because of a broken inversion symmetry but cause a different behaviour in the resulting sub-cycle dynamics. An interesting question is whether something is to be gained by combining the two. One possibility is to extend the harmonic cutoff by suppressing the system-induced gating of an oriented polar molecule using field-induced gating as in figure 3.6(a). The combined effect is to suppress tunnelling into the continuum in both half-cycles, thus suppressing both HHG and ionization. Ionization of the target medium is one of the main restrictions in attaining high cutoffs as it causes depletion of the target medium as well as defocusing of the laser pulse due to free electrons. As a proof-of-principle calculation we have used MO-ADK theory [38, 39] to calculate the ionization rates for oriented CO with and without the added second harmonic, confirming a suppressed ionization rate. According to the MO-ADK calculations an electric field with a peak intensity of  $2.4 \times 10^{14}$  W/cm<sup>2</sup> with 1% added second

## Extending the harmonic cutoff

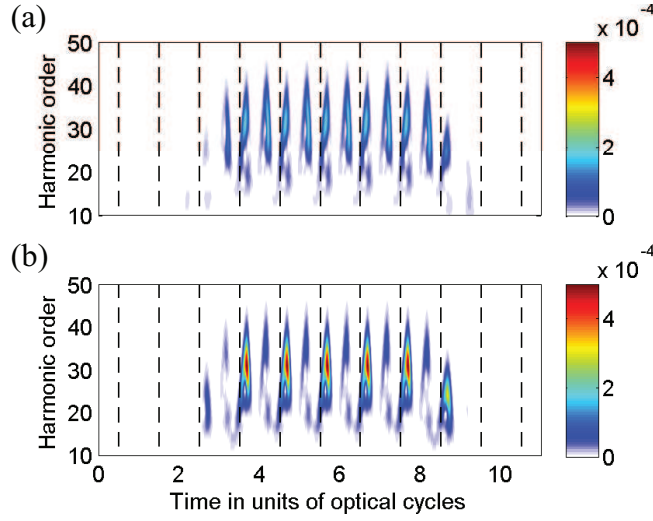


**Figure 3.6** | Gabor analysis illustrating the different dynamics of opposite orientations in field-induced gating. The total response of the aligned molecule is the coherent sum of the two orientations. The electric field is the one shown in figure 3.5. (a) The HOMO dipole is oriented in the positive  $x$  direction as in figure 3.1. The Gabor analysis would be the one shown in figure 3.4 in the absence of the second harmonic so the field-induced gating clearly counteracts the system-induced gating. (b) The HOMO dipole is oriented in the negative  $x$  direction causing the field-induced gating to enhance the system-induced gating.

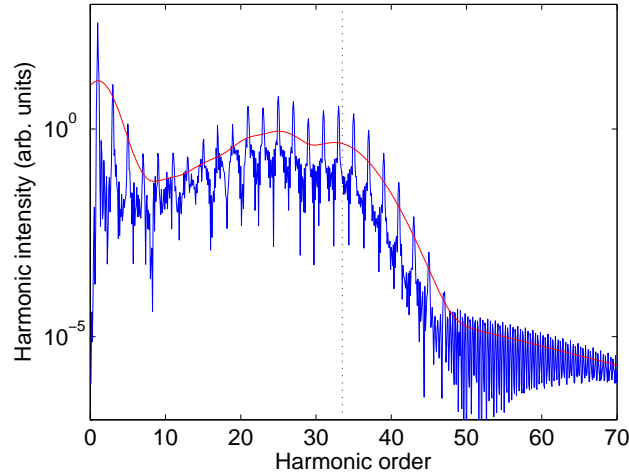


**Figure 3.7** | Reference HHG spectrum from aligned CO calculated with the Stark shift included in (2.6) as dictated by (3.6). The electric field is an 800 nm pulse with eleven optical cycles and a trapezoidal envelope with five optical cycles in the plateau. The peak intensity is  $2.0 \times 10^{14}$  W/cm<sup>2</sup>. Only odd harmonics appear due to the inversion symmetry of both target and field. The smooth (red) curve is obtained by averaging over neighbouring peaks. The vertical broken line indicates the harmonic cutoff calculated using  $\omega_{\max} = I_p + 3.17U_p$ . The Stark effect is not included in estimating the cutoff.

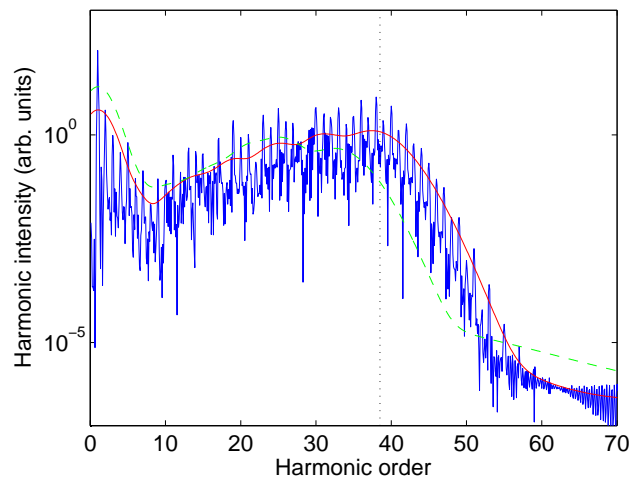


**Figure 3.8** | HHG spectrum illustrating the extension of the harmonic cutoff in a combined system-induced and field-induced gating scheme. The target CO molecule is oriented as in figure 3.1. The two-colour field is chosen so as to counteract the system-induced gating, resulting in a reduced ionization rate as described in the text. Using the combined gating scheme the peak intensity of the 800 nm component can be raised to  $2.4 \times 10^{14}$  W/cm<sup>2</sup> before the ionization rate is the same as in figure 3.7. The vertical dashed line indicates the harmonic cutoff calculated using  $\omega_{\max} = I_p + 3.17U_p$ . The Stark effect and the second harmonic are not included in estimating the cutoff. The dashed (green) line is the smoothed spectrum from figure 3.7.

harmonic causes the same amount of ionization as the original single-colour field with a peak intensity of  $2.0 \times 10^{14}$  W/cm<sup>2</sup>.

Our reference spectrum at  $2.0 \times 10^{14}$  W/cm<sup>2</sup> is shown in figure 3.7. The double gating scheme spectrum is shown in figure 3.8. Comparison shows an increase in cutoff of roughly five harmonic orders, corresponding to a 14% extension. This increase can be entirely ascribed to the higher intensity of the 800 nm component of the driving field using a semi-classical cutoff rule.



---

## Conclusions and outlook

### 4.1 Conclusions

The theory and results discussed in this progress report sum up the research performed during the first half of my PhD studies. My initial work centered on the importance of using the extended saddle-point method when evaluating the Lewenstein model of HHG. We discovered that using the extended saddle-point method is important when calculating the ellipticity of high-order harmonics emitted from aligned molecules. The reason for this is that the extended saddle-point method includes semi-classical orbits in which an electron is ionized at one atomic centre and recombines at another. The effect on the ellipticity is not large enough to entirely explain experimental data but it does present an example in which a correlation between ionization site and recombination site plays a role. This is interesting as several models of HHG factor away any correlation between the ionization step and the recombination step.

The second part of my work is about the importance of including the effect of the driving field on the molecular ground state. The standard Lewenstein model only models the free-electron motion in the laser field, and therefore cannot account for such an effect. We include the laser interaction by Stark shifting the individual molecular orbitals in a quasi-static approximation. This gives rise to a time-dependent ionization potential, which breaks the symmetry between neighbouring half-cycles for an oriented molecule.

### 4.2 Outlook

Based on my previous work there are several interesting lines of inquiry. Here we shall consider a few of them.

### 4.2.1 Structure determination for polar molecules

A major topic of interest in HHG is the identification of features in the harmonic spectrum, which map back to the geometry of the target molecule. The most successful model is the two-centre interference model. The main idea is that each nuclear site serves as a point emitter in the recombination step. The total emission then resembles that in a Young's double slit experiment. Destructive interference is obtained for certain frequencies depending on the internuclear separation. These minima have been observed both experimentally and in model calculations. There is, however, much interest in extending the sophistication of the possible structure predictions. In the case of polar molecules the two nuclei are no longer the same. This translates into a case where the two point emitters no longer have the same strength. The exact impact of this on the harmonic spectrum has not been treated. We would be able to address this question using our extended Lewenstein model for polar molecules. Our group has also recently finished a piece of code that solves the time-dependent Schrödinger equation on a grid in an effective single-electron potential. It is an extension of the strong-field ionization code developed by Thomas Kim Kjeldsen, and has already yielded interesting results on the two-centre model for homonuclear molecules. An extension to polar molecules would complement the Lewenstein results nicely.

### 4.2.2 Full momentum integral

Our work on elliptically polarized high-order harmonics shows that it can be important to include more orbits than the one obtained using the standard stationary-phase method. It is also commonly known that the standard treatment of the Lewenstein model fails to describe the harmonic signal when the polarization axis of the driving laser lies in a nodal plan of the molecular orbital. Solutions of the time-dependent Schrödinger equation (TDSE) show that in this case it is actually orbits that have a non-vanishing angle to the laser polarization that will dominate. It is therefore of interest to have an effective implementation of the full Lewenstein model. One such implementation reduces the three-dimensional momentum integral to a one-dimensional integral using the generalized Feynman identity [17].

The basis states used by quantum chemistry programs are polynomials times a Gaussian. The reason for this is that then all matrix elements are analytically known. As our code takes these basis states as input, it is possible to use the same trick when evaluating the three-dimensional momentum integral in the Lewenstein model. This could give calculation times which are even shorter than those in [17]. With this code we could systematically compare the effect of including only the standard orbit, exchange orbits or all orbits. An interesting test case would be to investigate the importance of the additional orbits in the prediction of elliptically polarized harmonics.

It would also be of interest to run a detailed comparison with our TDSE tool in order to fully characterize the predictive power of the full Lewenstein model. If the Lewenstein model yields good results, then it could be applied as input code

in studies on propagation effects in the target medium. The appeal of using the Lewenstein model rather than the TDSE solver is that such propagation studies are very time-consuming.

### 4.2.3 Propagation in the medium

Most theoretical work on HHG is done on single atoms or molecules. Extending the treatment to include propagation in the target medium is numerically very demanding. For atomic targets this has been done by calculating the single-atom responses in parallel, and propagating the driving field and the generated harmonics on a master node [40]. We have planned a research stay for me at Louisiana State University, where Mette Gaarde will introduce me to their parallel code. The plan is that I get to work on extending it to molecules. The main issue is to make the single-molecule calculations effective enough. My own Lewenstein code with the full momentum integral might serve this purpose.

Exciting research possibilities in this field include structuring the medium in various ways. The main goal of this would be to obtain quasi phase-matching in order to increase the obtainable output intensity of the generated attosecond pulse. Structures could include variations in density, alignment or orientation. These variations could be combined with variations in laser intensity, polarization or waveform.



---

## Bibliography

- [1] A. Etches, C. B. Madsen, and L. B. Madsen, *Phys. Rev. A* **81**, 013409 (2010).
- [2] A. Etches and L. B. Madsen, *J. Phys. B* (2010).
- [3] M. Lewenstein, P. Balcou, M. Y. Ivanov, A. L'Huillier, and P. B. Corkum, *Phys. Rev. A* **49**, 2117 (1994).
- [4] J. Levesque, Y. Mairesse, N. Dudovich, H. Pépin, J.-C. Kieffer, P. B. Corkum, and D. M. Villeneuve, *Phys. Rev. Lett.* **99**, 243001 (2007).
- [5] X. Zhou, R. Lock, N. Wagner, W. Li, H. C. Kapteyn, and M. M. Murnane, *Phys. Rev. Lett.* **102**, 073902 (2009).
- [6] P. B. Corkum, *Phys. Rev. Lett.* **71**, 1994 (1993).
- [7] C. C. Chirilă and M. Lein, *J. Mod. Opt.* **54**, 1039 (2007).
- [8] C. B. Madsen and L. B. Madsen, *Phys. Rev. A* **74**, 023403 (2006).
- [9] C. B. Madsen, A. S. Mouritzen, T. K. Kjeldsen, and L. B. Madsen, *Phys. Rev. A* **76**, 035401 (2007).
- [10] C. B. Madsen and L. B. Madsen, *Phys. Rev. A* **76**, 043419 (2007).
- [11] C. B. Madsen, Master's thesis, Aarhus Graduate School of Science (2008).
- [12] C. B. Madsen, M. Abu-samha, and L. B. Madsen, *Phys. Rev. A* **81**, 043413 (2010).
- [13] R. N. Zare, *Angular momentum: understanding spatial aspects in chemistry and physics* (John Wiley, New York, 1987).

## Bibliography

- [14] M. Schmidt, K. Baldrige, J. Boatz, S. Elbert, M. Gordon, J. Jensen, S. Koseki, N. Matsunaga, K. Nguyen, S. Su, et al., *J. Comput. Chem.* **14**, 1347 (1993).
- [15] C. C. Chirilă and M. Lein, *Phys. Rev. A* **73**, 023410 (2006).
- [16] M. Lein, N. Hay, R. Velotta, J. P. Marangos, and P. L. Knight, *Phys. Rev. Lett.* **88**, 183903 (2002).
- [17] C. C. Chirilă and M. Lein, *Phys. Rev. A* **80**, 013405 (2009).
- [18] M. Born and E. Wolf, *Principles of Optics: Electromagnetic Theory of Propagation, Interference and Diffraction of Light* (Pergamon Press, 1970), 4th ed.
- [19] M. Lein, N. Hay, R. Velotta, J. P. Marangos, and P. L. Knight, *Phys. Rev. A* **66**, 023805 (2002).
- [20] O. Smirnova, S. Patchkovskii, Y. Mairesse, N. Dudovich, D. Villeneuve, P. Corkum, and M. Y. Ivanov, *Phys. Rev. Lett.* **102**, 063601 (2009).
- [21] A.-T. Le, R. R. Lucchese, S. Tonzani, T. Morishita, and C. D. Lin, *Phys. Rev. A* **80**, 013401 (2009).
- [22] C. C. Chirilă and M. Lein, *Phys. Rev. A* **77**, 043403 (2008).
- [23] L. Holmegaard, J. L. Hansen, L. Kalhøj, S. L. Kragh, H. Stapelfeldt, F. Filsinger, J. Küpper, G. Meijer, D. Dimitrovski, M. Abu-samha, et al. (2010), URL [arXiv:1003.4634v1](https://arxiv.org/abs/1003.4634v1).
- [24] T. Kreibich, M. Lein, V. Engel, and E. K. U. Gross, *Phys. Rev. Lett.* **87**, 103901 (2001).
- [25] H. Stapelfeldt and T. Seideman, *Rev. Mod. Phys.* **75**, 543 (2003).
- [26] S. De, I. Znakovskaya, D. Ray, F. Anis, N. G. Johnson, I. A. Bocharova, M. Margravelidze, B. D. Esry, C. L. Cocke, I. V. Litvinyuk, et al., *Phys. Rev. Lett.* **103**, 153002 (2009).
- [27] L. Holmegaard, J. H. Nielsen, I. Nevo, H. Stapelfeldt, F. Filsinger, J. Küpper, and G. Meijer, *Phys. Rev. Lett.* **102**, 023001 (2009).
- [28] G. L. Kamta and A. D. Bandrauk, *Phys. Rev. Lett.* **94**, 203003 (2005).
- [29] N. Dudovich, O. Smirnova, J. Levesque, Y. Mairesse, M. Ivanov, D. Villeneuve, and P. Corkum, *Nature Physics* **2**, 781 (2006).
- [30] T. Pfeifer, L. Gallmann, M. J. Abel, D. M. Neumark, and S. R. Leone, *Opt. Lett.* **31**, 975 (2006).
- [31] J. Mauritsson, J. M. Dahlström, E. Mansten, and T. Fordell, *J. Phys. B.* **42**, 134003 (2009).

## Bibliography

- [32] P. Antoine, B. Piraux, and A. Maquet, *Phys. Rev. A* **51**, R1750 (1995).
- [33] C. C. Chirilă, I. Dreissigacker, E. V. van der Zwan, and M. Lein, *Phys. Rev. A* **81**, 033412 (2010).
- [34] G. L. Kamta and A. D. Bandrauk, *Phys. Rev. A* **70**, 011404 (2004).
- [35] E. Goulielmakis, M. Schultze, M. Hofstetter, V. S. Yakovlev, J. Gagnon, M. Uiberacker, A. L. Aquila, E. M. Gullikson, D. T. Attwood, R. Kienberger, et al., *Science* **320**, 1614 (2008).
- [36] N. Dudovich, J. Levesque, O. Smirnova, D. Zeidler, D. Comtois, M. Y. Ivanov, D. M. Villeneuve, and P. B. Corkum, *Phys. Rev. Lett.* **97**, 253903 (2006).
- [37] H. Mashiko, S. Gilbertson, C. Li, S. D. Khan, M. M. Shakya, E. Moon, and Z. Chang, *Phys. Rev. Lett.* **100**, 103906 (2008).
- [38] X. M. Tong, Z. X. Zhao, and C. D. Lin, *Phys. Rev. A* **66**, 033402 (2002).
- [39] T. K. Kjeldsen and L. B. Madsen, *Phys. Rev. A* **71**, 023411 (2005).
- [40] M. B. Gaarde, J. L. Tate, and K. J. Schafer, *J. Phys. B* **41**, 132001 (2008).